Journal of Hydrology: Regional Studies 62 (2025) 103021

Contents lists available at ScienceDirect

Journal of Hydrology: Regional Studies

journal homepage: www.elsevier.com/locate/ejrh

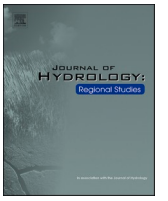

Impact of global warming on precipitation extremes based on the design frequencies over South Korea

Ana Juzbašić [a], Changyong Park [a,*], Dong-Hyun Cha [a,*], Joong-Bae Ahn [b], Eun-Chul Chang [c], Seung-Ki Min [d], Youngeun Choi [e], Young-Hwa Byun [f]

[a] Department of Civil, Urban, Earth and Environmental Engineering, Ulsan National Institute of Science and Technology, Ulsan, Republic of Korea
[b] Department of Atmospheric Sciences, Pusan National University, Busan, Republic of Korea
[c] Department of Atmospheric Science, Kongju National University, Kongju, Republic of Korea
[d] Division of Environmental Science and Engineering, Pohang University of Science and Technology, Pohang, Republic of Korea
[e] Department of Geography, Konkuk University, Seoul, Republic of Korea
[f] National Institute of Meteorological Sciences, Seogwipo, Republic of Korea

ARTICLE INFO

Keywords:
Return value
Climate change
South Korea
Bias correction
Extreme precipitation

ABSTRACT

Study region: South Korea (SK), East Asia
Study focus: The increasing number and intensity of precipitation make South Korea highly vulnerable to climate change. Therefore, accurate predictions of future extreme events are essential for this region. In the present study, we demonstrate that the models have some significant biases in the projection of precipitation extremes and that the bias correction using quantile delta mapping resolves most of these issues. Additionally, the future projections of extreme precipitation are analyzed by using the generalized extreme value theory.
New hydrological insights for the region: The present study demonstrates that the values associated with specific return periods are projected to increase, signifying intensification of precipitation and the higher likelihood of the extreme events occurring in the future. Therefore, it is of utmost importance to consider using forecasted future design frequencies instead of ones based on the historical record when planning the flood defenses and agricultural development.

1. Introduction

South Korea (SK) is a region vulnerable to precipitation extremes, a consequence of the geographical location making it in the path of tropical cyclones, the East Asian Summer Monsoon (EASM) rain band, and heavy convective rains in the summer season. SK is vulnerable to major hazards related to extreme precipitation, such as flooding and landslides, which can cause both economic damage and loss of human lives. From 1984–1990, South Korea experienced severe flood and typhoon damage, including more than 360,000 victims in the Seoul metropolitan region in 1984 and over 200,000 victims with approximately 770 million USD in losses in 1990. The most destructive disaster in the past 35 years was Typhoon *Rusa* in 2002, which caused over 6.15 billion USD in damages. Typhoon *Maemi* in 2003 and *Ewiniar* in 2006 followed, causing losses of approximately 4.6 billion USD and 1.5 billion USD, respectively (National Geographic Information Institute, 2020). Another particularly notable event occurred in 2011, when a landslide was triggered by a 120-year return period rainfall event on Mt. Umyeon (Umyeonsan) in the Gangnam district of Seoul, resulting in significant

* Corresponding authors.
E-mail addresses: parkcy@unist.ac.kr (C. Park), dhcha@unist.ac.kr (D.-H. Cha).

https://doi.org/10.1016/j.ejrh.2025.103021
Received 8 January 2025; Received in revised form 5 November 2025; Accepted 3 December 2025
Available online 6 December 2025

casualties and drawing nationwide attention (Seoul Metropolitan Government, 2014). More recently, SK has continued to experience a series of extreme precipitation events – the 2020 flooding that resulted in 46 casualties and significant economic loss (KMA, 2021), where the heaviest daily precipitation ever recorded occurred; the extreme rainfall in August of 2022, which has caused severe flooding in the Seoul region (Sung et al., 2023), as well as damage to the photovoltaic power plant in Gangwon province (Lee et al., 2023), directly followed by the landfall of typhoon *Hinnamnor*, which resulted in eleven casualties and around 200 million USD in damages (Ministry of the Interior and Safety, 2023). The intensity and frequency of precipitation extremes have been increasing due to the effects connected to global and regional climate change (IPCC, 2014; 2022). Namely, both the intensity of typhoons affecting SK and the intensity of the East Asian Summer Monsoon (EASM) have been increasing (Baek et al., 2017; Lee et al., 2023).

While they are widely used and provide an overall good picture of the projected future climate, global climate models (GCMs) have a drawback in the way of relatively coarse resolution, which is insufficient for more detailed descriptions of local impacts. Therefore, to address the changes on more regional scales, and especially in the regions of complex topography where the effect of local-to-regional scale forcing is pronounced, regional climate models (RCMs) are necessary (Kim et al., 2020; Torma et al., 2015). The added value provided by dynamical or statistical downscaling of the GCM output by RCMs has been especially shown to be noticeable for the tail-ends (that is, extremes) of the distributions (Ciarlo``` et al., 2021; Lee and Hong, 2014), making RCM projections useful for the analysis of extremes in the SK region.

The East Asia phase II domain of the Coordinated Regional Climate Downscaling Experiment (CORDEX; https://cordex.org/) encompasses the SK as well as the wider East Asian region. The data produced as part of this project has been previously utilized for analysis of the rainfall in the whole East Asia domain (Park et al., 2020; Seo et al., 2023), as well as smaller localized studies for the Korean Peninsula (Kim et al., 2020; Park et al., 2022).

However, raw projection data from the models have some inherent biases, due to imperfect numerical schemes, parametrizations, and modeling mechanisms in general, which is especially noticeable in the simulations of the extremes (Chen et al., 2021). Therefore, bias correction techniques are usually applied to improve simulations. While there is a wide variety of bias correction methods available, different variations of quantile mapping are the ones most used for the correction of precipitation (Cannon et al., 2015; Kim et al., 2020; Ngai et al., 2017)

As the climate further changes, the precipitation extremes are projected to intensify even more (IPCC, 2022). Especially, several recent analyses of the future projections of summer precipitation have shown that Asian monsoon precipitation is expected to increase (Li et al., 2019; Moon and Ha, 2020). Therefore, the danger of flooding and landslides is also projected to increase in the future. To prepare for potential future disasters, accurate projections of extremes need to be provided to policymakers and risk modelers. In the case of precipitation, return values and/or return periods (Gumbel, 1941) are intuitively understood and commonly used in hydrology, risk assessment, and hydro-power projections. However, the current use of return periods and values associated with them for these fields is commonly limited to the ones calculated from the historical periods. In the changing climate, however, the return periods are also likely to change (Park and Min, 2019; Qin and Dai, 2022), making it paramount to consider the modeled values for the future climate.

Therefore, this study aims to provide insights into the bias in the precipitation projections over SK and the necessity of correcting such bias when precipitation extremes are concerned, as well as address the possible future changes in spatially detailed extreme precipitation events using a regional climate model under different emission scenarios.

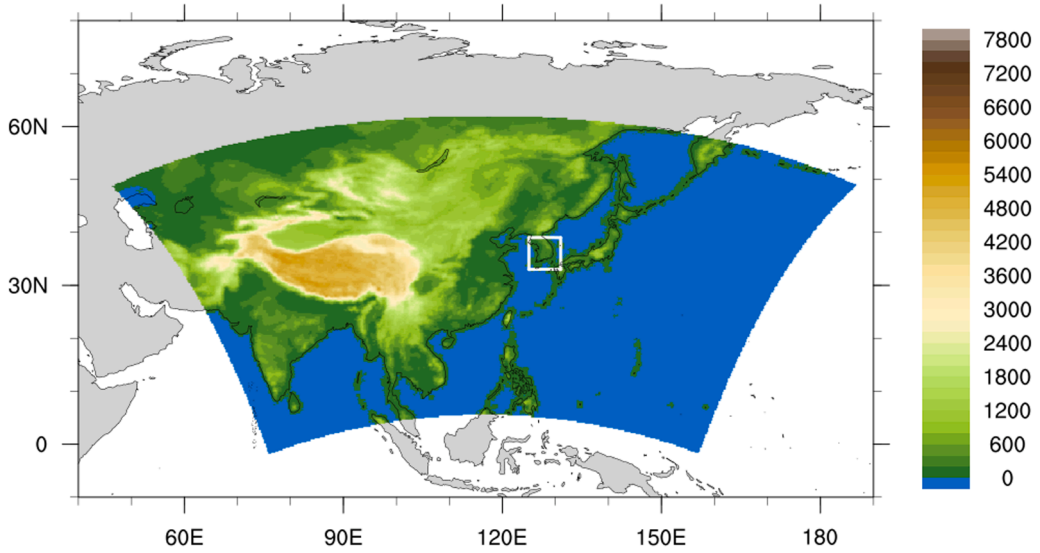

Fig. 1. CORDEX-EA simulation domain (colored) and the analysis domain (white rectangle). Each color indicates the altitude (unit: m).

2. Data and methods

2.1. Study region

The present study focuses on the region roughly corresponding to the territory of Republic of Korea (South Korea, SK), located on the southern part of the Korean Peninsula in East Asia. The study domain has been defined as 125–131°E, 33–39°N (white rectangle in Fig. 1). The peninsula is surrounded by the Yellow Sea in the west, Korea Strait in the south and the East Sea in the east, which significantly impact its climate. Topographically, SK is characterized by complex terrain, with roughly 70 % of the country covered by mountains, including Taebaek and Sobaek ranges, and a highly indented coastline.

According to Köppen–Geiger climate classification (Beck et al., 2018), Korean climate is mainly classified as Dwa (inland regions; monsoon-influenced hot-summer humid continental climate), Dfa (east and west coast; hot-summer humid continental climate) and Cfa (southern coast and Jeju Island; humid subtropical climate). SK experiences four distinct seasons: cold dry winters associated with Siberian high-pressure system, hot and wet summers under influence of East Asian Summer Monsoon (EASM), and mild spring and autumn seasons. Due to influence of EASM and the convective rains, summer months (June-August) contribute 50–60 % of the annual precipitation.

2.2. Data

This study was conducted using daily precipitation data for the boreal summer period (June–July–August (JJA)), as this is when most precipitation extremes occur in this area. Asian Precipitation - Highly-Resolved Observational Data Integration Towards Evaluation of Water Resources (APHRODITE) (Yatagai et al., 2012) dataset on the 0.25 × 0.25° grid was utilized for bias correction and evaluation of model performance. The APHRODITE dataset is a gridded daily product derived from the long-term (1951 onward) records from a dense network of rain gauges in Asia. Therefore, in the remainder of the study, we refer to it as "observation". As the APHRODITE does not include precipitation over the ocean, only the modeled data over land was used in this study.

The present study also makes use of the model data from fifteen different GCM-RCM chains. The aforementioned data were produced as part of the CORDEX-EA Phase II project. The combinations include four total GCMs, three (GFDL-ESM-2M (Geophysical Fluid Dynamics Laboratory Earth System Model (Dunne et al., 2012)), HadGEM2-AO (Hadley Centre Global Environment Model version 2 – Atmosphere-Ocean (Martin et al., 2011)), and MPI-ESM-LR (Max Planck Institute Earth System Model Low Resolution (Giorgetta et al., 2013)) from Coupled Model Intercomparison Project Phase (CMIP) phase 5, using representative concentration pathway (RCP) scenarios; and one (UKESM (UK Earth System Model (Sellar et al., 2019)) from the CMIP phase 6, using shared socioeconomic pathway (SSP) scenarios. These GCM outputs were dynamically downscaled using six different RCMs. The GCM-RCM chains, their resolutions, and parametrizations are listed in Table 1. The models were run on a curvilinear grid, which was regridded using bilinear interpolation to the observational grid (0.25x0.25°) for ensembling and comparison. The models were run for the period from 1979 to 2099 (or 2100, depending on the model). Four different 25-year periods were chosen for the analysis – the historical period running from 1981

Table 1
RCM settings and parametrizations.

RCM	Parametrizations					CGCMs downscaled	Resolution and number of grid points (lat x lon)	RCM reference
	Convection Parameterization Schemes	Microphysics	Radiation	Land Surface Model	Planetary Boundary Layer			
WRF v.4	Betts–Miller–Janjic	WSM3	Community Atmospheric Model radiation scheme (CAM)	NOAH	Yonsei University (YSU) PBL	GFDL-ESM2M MPI-ESM-LR UK-ESM	25 km, 250 × 395	Gochis et al. (2017)
RegCM v.4	MIT–Emanuel	SUBEX	NCAR CCM3	NCAR CLM3.5	Holtslag	GFDL-ESM2M, HadGEM2-AO UK-ESM	25 km, 249 × 394	Giorgi et al. (2012)
MM5 v.5	Kain and Fritsch	Reisner II	CCM2 radiative transfer scheme	CLM3	YSU	HadGEM2-AO MPI-ESM-LR	25 km, 260 × 405	Grell et al. (1994)
CCLM v.5	Tiedke	Extended DM	Ritter and Galeyn	TERRA ML	Davies and Tumer	HadGEM2-AO MPI-ESM-LR UK-ESM	25 km, 231 × 376	Doms, G., and Baldauf, M., (2013)
HadGEM3-RA	Revised mass flux	Single moment bulk	General 2-stream radiation	Joint UK Land Environment Simulator (JULES)	Smith (1990), Lock et al. (2000)	HadGEM2-AO, MPI-ESM-LR, UK-ESM	25 km, 251 × 396	Davies et al. (2005)
GRIMs	Simplified Arakawa–Schubert	WSM1	LW: Chou, SW: Chou and Suarez	NOAH	YSU PBL	UK-ESM	25 km, 252 x 401	Hong et al. (2013)

to 2005, and the near (2025–2049), middle (2050–2074), and far future (2075–2099). Within the CORDEX-EX phase II project the models were run for four RCP scenarios – RCP2.6, RCP4.5, RCP6.0, and RCP8.5, where numbers represent the radiative forcing in 2100, and four SSP scenarios – SSP1–2.6, SSP2–4.5, SSP3–7.0 and SSP5–8.5, where the first number represents the type of scenario, while the second number represents the radiative forcing.

For model performance analysis, each model has first been analyzed separately. Then, the models were combined into multi-model-ensembles (MME) according to the scenarios used. It is a commonly used method that has been proven to decrease bias and improve overall performance in numerous previous studies (Im et al., 2017; IPCC, 2014; Park et al., 2020; Seo et al., 2023). Because the corresponding RCP and SSP scenarios are similar, with SSP being based on RCP, they have been combined into "low emission" (RCP2.6 and SSP1–2.6) and "high emissions" (RCP8.5 and SSP5–8.5) MME. These specific scenarios were selected as they represent the low and high ends of the emission scenario spectrum.

2.3. Methods

A number of studies have demonstrated the usefulness of bias correction in future projections. Several of these studies have shown that quantile mapping is the most appropriate method for correcting biases in precipitation simulations (Cannon et al., 2015; Kim et al., 2020; Ngai et al., 2017; Qin and Dai, 2022). Various quantile mapping methods exist, including general quantile mapping (usually referred to as quantile mapping, QM), detrended quantile mapping (DQM), empirical quantile mapping (EQM), and quantile delta mapping (QDM). The main benefit of using QDM over other methods is the lack of the need for extrapolation, as this method preserves the modeled changes explicitly, whereas other methods can lead to artificial inflation of future projections. The QDM algorithm used in the present study, developed by Cannon et al. (2015), consists of the following steps described in Fig. 2. First, the modeled changes in quantiles are calculated. Then, the modeled data is detrended by quantile, and the historical data is bias corrected. Following bias correction, the modeled changes are added back multiplicatively, explicitly preserving the modeled changes. This correction method was applied separately to daily data at each grid point for each model.

In the present study, the return value for several periods has been chosen as the indication of extreme precipitation. In the present research, the block maxima approach (or generalized extreme value, GEV approach) was chosen, as this is a method commonly used in hydrology, making it most useful for future flood risk analysis (Jesus et al., 2020; Katz et al., 2002; Morrison and Smith, 2002; Nyaupane et al., 2018.; Vangelis et al., 2022). The return value refers to the amount of heavy rain that is expected to occur during a certain period of time, which is referred to as the return period. For example, a precipitation level with a return period of 100 years means that the event will occur with a probability of 1/100 each year. Additionally, this method has a very intuitive interpretation and, by design, avoids the clustering (phenomenon in which several values from the same event are interpreted as different values/events) issue that can happen with different approaches. The block maxima approach begins with choosing a time block – in the present study, a block chosen was a period of one year. Therefore, the values used as a basis for GEV analysis were the maximum daily precipitation (Rx1d). The GEV distribution, by definition, has three forms: Gumbel (type I), Fréchet (type II), and Weibull (type III), however precipitation and flooding, in general, follow the Gumbel distribution (Gumbel, 1941). The return periods and values corresponding to them are then extracted from the fit of the Rx1d values to the GEV distribution at each grid point. As the assumption of stationarity is likely to break with longer periods of data, especially considering climate change impact, each period analyzed in this study was fitted to GEV distribution separately. In the present study, while we do analyze all of the return periods to some extent, return values of 30 and 100 years were chosen for more detailed analysis. Historically the values of 10 and 30 years were used for the design frequencies of flood drains in SK (Government of the Republic of Korea, 2020), however, due to the changing climate, the guidelines are likely to include longer periods in the future. As noted in Chapter 1, rainfall events with return values exceeding 100 years have been occurring with increasing frequency in recent years. In addition, the design frequencies of flood drainage systems have been revised upward at

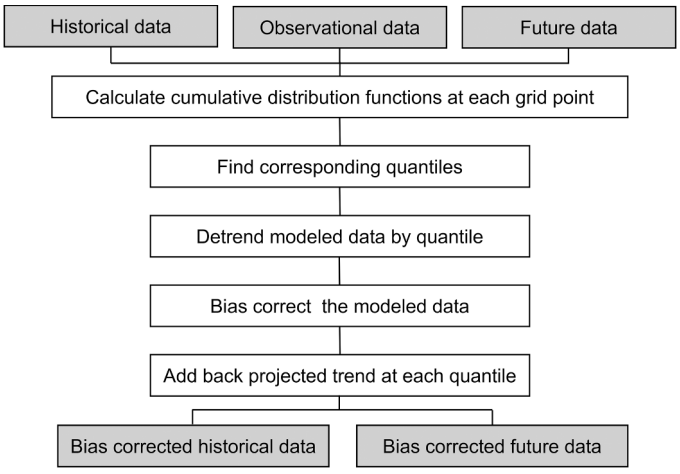

Fig. 2. Flow chart showing the procedure of quantile delta mapping.

the national level. As climate changes and extreme events happen unpredictably, the value of 100 years is analyzed in this study as the reference point.

3. Results

3.1. Performance of the models and the necessity of bias correction

First, we analyzed the performance of each model both before and after bias correction for the Rx1d averaged for the historical period (1981–2005). The results of this analysis are shown in Fig. 3. Most of the models show a similar pattern of errors before bias correction. That is, most models show the overestimation of Rx1d over the north-western part of the SK and coastal regions in the south-eastern part, with an underestimation of precipitation amount in the south-western inland part of the SK. Notably, there are some differences between models. For example, some of the models have a larger wet bias; the UKESM-GRIMS chain overestimates the precipitation over the whole SK, and so does HG2_MM5, but to a lesser extent. Additionally, MPI_WRF has a larger dry bias over the southeastern part of the SK than other models. The bias averaged over the whole region ranges from −9.4 % (MPI_WRF chain) to + 48.1 % (UKESM_GRIMS chain). MME results in a bias of 8.3 %, with the large wet bias on the northwestern part of the analysis domain and dry bias in the southwestern part canceling each other to a certain extent.

After bias correction has been performed, the area-averaged bias ranges between −3.5 % (HG2_REGCM) and + 2.4 % (UKESM_-GRIMS). However, notably, both positive bias over the north-west and south-east parts and the dry bias over the south-east part of the analysis domain have been significantly reduced, with the remaining bias being under 10 % over the whole region, while in some regions before bias correction bias was above 100 %. After bias correction, the performance of all models, and especially MME, which has a bias of 0.1 %, is sufficient for further analysis. A similar bias analysis has been performed for other mean and extreme indices (namely, mean precipitation, maximum continuous 5-day precipitation, simple daily intensity index, and number of days over 20 mm; not shown), with similar results of very little (or none in case of mean) bias remaining after bias correction.

Additionally, one of the strengths of QDM as a bias-correction method is its ability to keep the variability in line with historically observed ones, as the method explicitly corrects bias in each quantile and adds modeled changes in each quantile at the end. In the present study, the variance of the original modeled and bias corrected data was calculated and compared to the observation, and the results are shown in Table 2. The same methodology used for calculating averages is employed here, that is, variances (standard deviations) are calculated separately for each model at each grid point, prior to averaging or ensembling.

For the SK area, in observational dataset, the recorded grid-point interannual variance ranges between 171.28 and 3545.06 (standard deviations of 13.09–59.54). However, the modeled variance before bias correction varies between 304.46 and 26155.60 (standard deviation of 17.45–161.72). That is, both the grid points with lower and higher variance have much higher modeled variance than the observed one, indicating models overestimate variability of precipitation as well as overestimating means. Bias correction helps align the model output with the observed inter-annual variability. Averaged over the whole analyzed domain, the observed variance was 1001.63 (std 30.47. In contrast, the original modeled variances were significantly higher, ranging from 1350.35 to 2824.93 (std 35.86–51.68), depending on the model. After applying QDM on the daily values and calculating Rx1d, the area averaged variance falls between 992.01 and 1160.51 (std 30.04–32.57). Thus, bias correction effectively improves the representation of interannual variance in extreme values as well as improving the means.

Finally, to avoid any artificial reductions in variability, all the ensembling in the current study has been done as the last step of the analysis.

We present the comparison of the return values (RVs) associated with specific periods for the SK average calculated from the original model projections and the bias-corrected data in Fig. 4. The spread between different models for the same period and same scenario is much higher in the original (non-corrected) values. However, bias correction decreases the inter-model spread by removing a model-specific bias, and then brings the model projections closer together indicating the consistency in the projections. Additionally, the original simulated RVs are often overestimated for the historical period. As the spread is quite high, some models underestimate the precipitation, leading to underestimating the potential dangers of extreme precipitation if those are used. Therefore, any future extreme precipitation projections need to be bias-corrected from the available model data and then ensembled.

To further the understanding of the historical patterns and the model performance for specific geographic locations, we have analyzed the historical observed and modeled values of 30-year (RV30) and 100-year (RV100) for each grid point (Fig. 5). As the need for bias correction has already been explained, we only show the results after bias correction. The largest precipitation amounts for all of the return periods were recorded in the western part of the southern coast (between 34 and 35°N, 126 and 127°E), Gangwon Province (36.5–38°N, 127–128°E) and Jeju Island (~33.25°N, 126.5°E). The western part of the southern coast and Gangwon Province are regions in South Korea that frequently experience heavy summer rainfall, as they are located along the typical landfall and exit tracks of typhoons affecting the Korean Peninsula. Typhoon *Rusa* in 2002 was associated with an extreme daily rainfall of 870.2 mm in Gangwon Province, representing one of the most intense rainfall events observed in Korea since records began. In addition, during summer, moist southerly winds often collide with Mt. Jiri(Jirisan), a high-elevation mountain near the southern coast, generating strong ascending air that frequently induces localized heavy rainfall on the windward side, particularly in the western part of the southern coast. In this region, an extreme case was observed on July 31, 1998, when 145.0 mm of precipitation was recorded within a single hour. Jeju Island, located further south, experiences the highest summer precipitation in South Korea, primarily due to its frequent exposure to both the EASM rainbands and typhoons. (Choi and Kim, 2007; National Geographic Information Institute, 2020; Park et al., 2008; 2022) The lowest were recorded in the northwestern part of the analysis domain, the current territory of North Korea (roughly around 38°N, 125–126°E). The RV30 values were between 80 and 224 mm, while those for the RV100 reached up to 269 mm

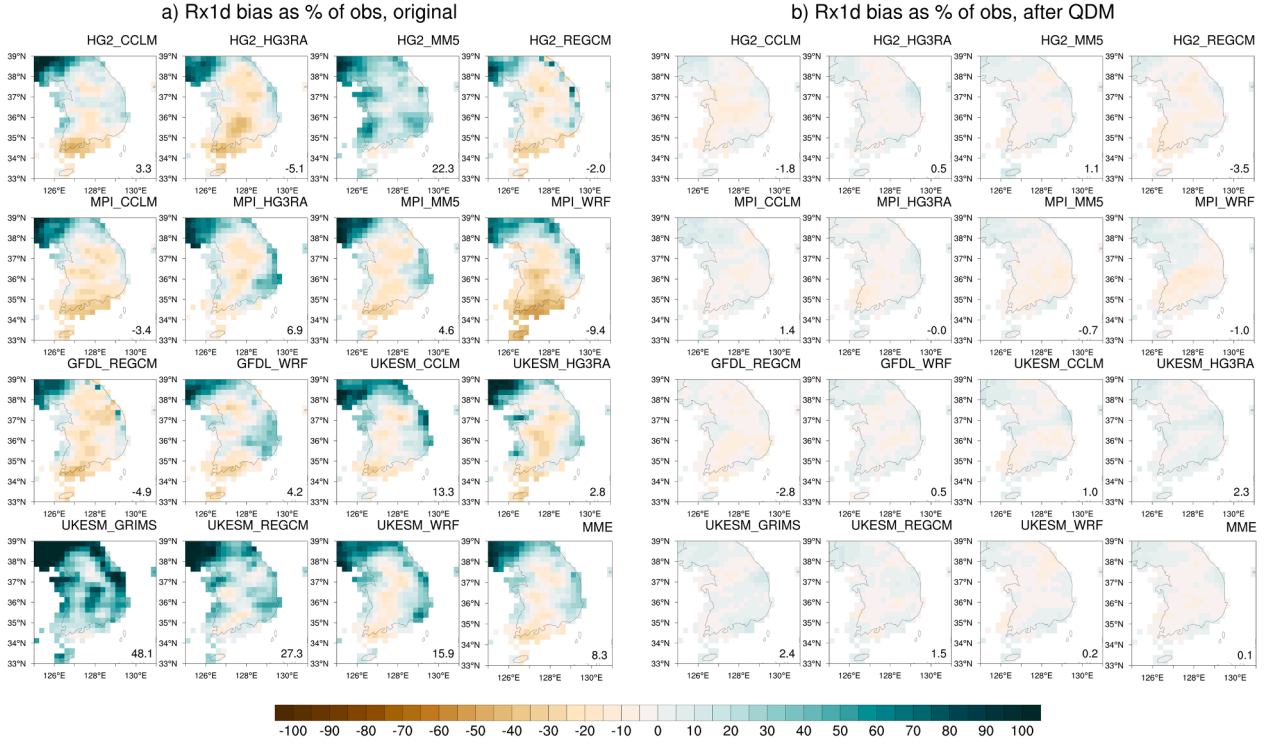

Fig. 3. Comparison of the bias (%) of the precipitation simulated in the models with the APHRODITE precipitation for raw model data (a) and after bias correction (b). The model chain is indicated above each panel.

Table 2
Variance (VAR, unit: mm^2) and standard deviations (STD, unit: mm) of Rx1d for observation (OBS), original modeled (ORG) and bias corrected (QDM) data. Minimum and maximum variance refer to individual grid points, while the ranges under SK refer to the minimum and maximum across models.

	VAR min and max	SK average VAR	SK average STD
OBS	171.28–3545.06	1001.63	30.47
ORG	304.46–26155.60	1350.35–2824.93	35.86–51.68
QDM	75.03 – 3388.28	992.01–1160.51	30.04–32.57

in the southern part of South Jeolla Province (~34.5°N, ~126.75°E). The bias for both periods was minor, at 1.1 % for RV30 and 1.4 % for RV100. Therefore, after bias correction, these simulations are appropriate for the analysis of the future changes in the precipitation extremes.

3.2. Future changes in the return values

In this chapter, we analyze the projected future changes in the return values. Fig. 6 shows the ensembled future changes of area-average return values (in mm) for SK for the return periods from 1 to 100 years. As the return periods get longer, the divergence of the higher emission scenario from the historical gets larger, indicating that there are higher increases for the extremes. This higher increase for longer periods and the divergence between low and high emission scenarios is more pronounced at the end of the century. Namely, while the low-emission scenarios indicate some increase, the curve of the projections follows the historical values, while the high-emission scenario diverges from the historical values more for the higher return periods. Fig. 7 shows a bar graph of the changes for some of the more commonly used return periods: 10,20,30,50 and 100 years. In the low emission scenario, the return values associated with these periods are projected to increase under or around 10 %, and the increase for all the periods analyzed in this study is very similar. In the mid-future period for low emission scenarios, the higher return periods are projected to increase slightly less than the lower return periods. However, for high emission scenarios, especially after mid-century, the higher return periods are associated with higher increases, that is, the RV100 at the end of the century is projected to increase more than other return values, implying the increase of the potential danger.

However, due to the nature of averaging, the details and some of the extremes can get lost. While the values averaged over SK provide a good base for understanding the changes of return values, to address more localized changes, we show the analysis of the changes of RV30 and RV100 for each grid point in Fig. 8. The general pattern of change is similar for both return periods analyzed; however, the increase is projected to be higher for RV100 in the higher emission scenarios for the whole region, indicating general intensification of extremes. In the low emission scenario, for both return periods, there is a slight increase or decrease projected, depending on the region, with the total area-averaged change being roughly 10 %. There are some regions in the northern part of the analysis domain that are projected to experience slightly more increase from mid-century, but the rest of the SK is not projected to experience significant increases in the return values in low-emission scenarios. For high-emission scenarios, however, the projected changes increase for both RV30 and RV100 as time goes by. In the near future (2025–2049), the projected increase is low over most of the domains, similar to the projections for low-emission scenarios. The difference between high and low emission scenarios starts being visible mid-century when especially southern coastal areas are projected to experience larger increases (around 30 %) in both RV30 and RV100. Additionally, it is already notable that the increase in RV100 is projected to be larger than the increase of RV30 by mid-century. This becomes even more distinct at the end of the century when the area-averaged RV30 is projected to increase by 35.8 %, while the RV100 is projected to increase by 38 %. The reason for slight differences in the area-averaged values between Figs. 7 and 8 is that for Fig. 7, as the purpose was to analyze the values area-averaged over the whole analysis domain, the area-averaging was done before calculating RVs, while for Fig. 8, where the purpose was to show the regional differences, the RVs were calculated at each grid point first, followed by their differences at those grid points, and then averaged over the domain, resulting in a minor discrepancy in the percentages, with the agreement of the trends. The return values are projected to increase the most in the coastal and lowland areas and less over the mountainous areas in the SK. That is, the cities with large populations such as Busan, Ulsan, and Daegu are likely to be affected by flooding caused by the increased precipitation more than the rural and mountainous areas closer to the center of the SK.

Finally, we address the likelihood of extreme events being exceeded. Fig. 9 shows all of the simulated Rx1d values as compared to the RV30 and RV100 of the same period. In the more extreme scenarios, especially around the end of the century, more of the projected Rx1d values are above RV30 (blue) and even above the RV100 (red) line. This implies that some projected Rx1d values exceed those generally predicted by simply fitting the Gumbel distribution, indicating a higher probability of unaccounted extremes. That is, while the Rx1d itself and the associated return values are projected to increase, which poses a significant threat in itself, the even bigger issue is that in the high emission scenario at the end of the century, there are several projected values that happen to be above the RV100. While not all models agree on those values, the possibility of these events increases as time goes by in the higher emission scenarios. This possibility of unaccounted extremes should, therefore, be taken into account when designing flood defense systems that are supposed to last for a long time. As the values associated with longer return periods are projected to increase even more, higher return periods should be chosen for the designs to avoid unaccounted-for extremes which have the potential for significant economic and human casualties. Additionally, given that even the projected value of RV30 at the end of the century is already higher than the value of historical RV100, and the significant number of events is projected to happen above this value (bottom right, Fig. 9), it is of utmost importance that the modeled, bias-corrected return values are used for the design of the long-term flooding solutions instead of

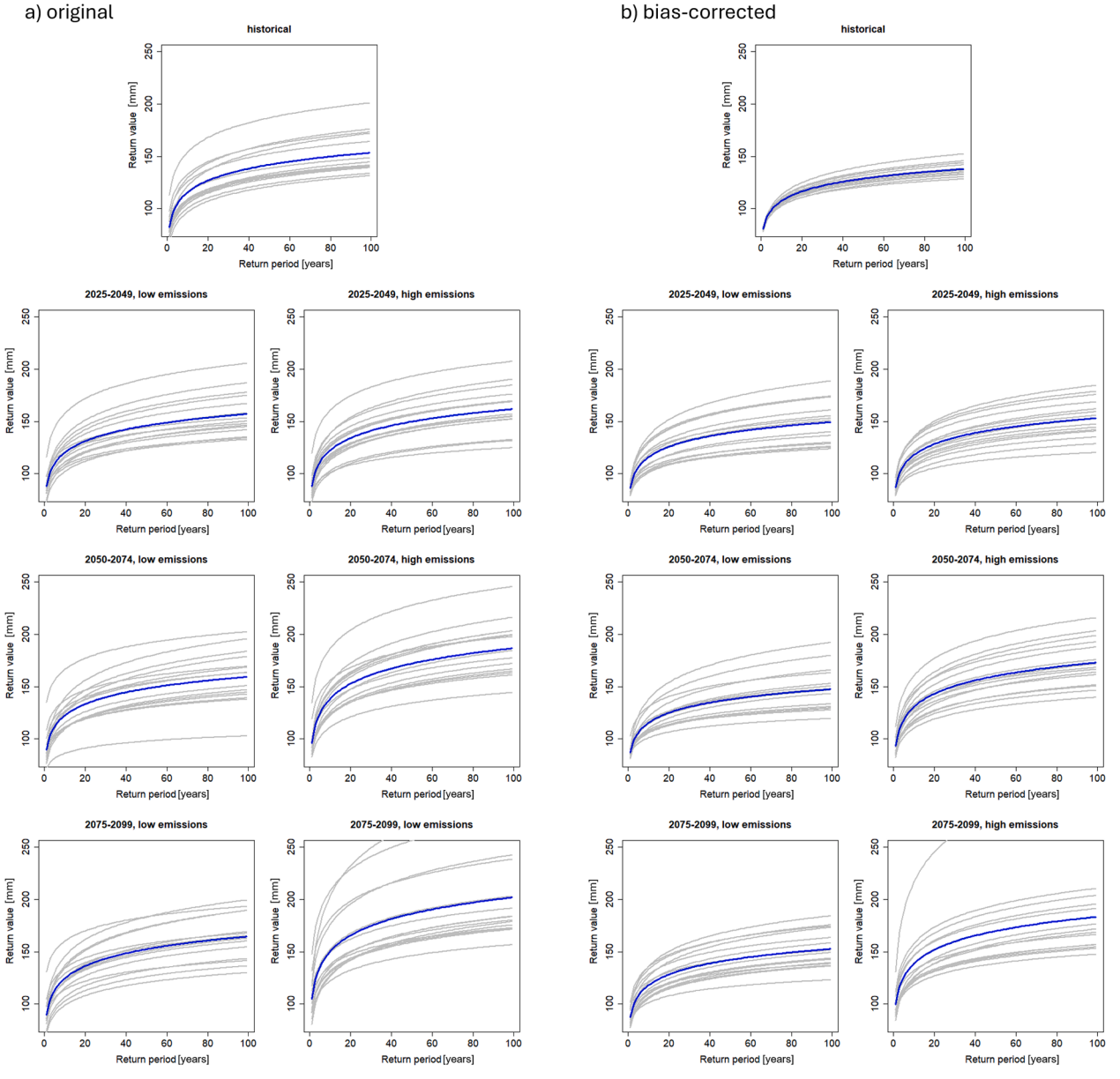

Fig. 4. The comparison of the simulated return values from the original data (a) and bias-corrected precipitation data (b). The blue line denotes the MME, while the grey lines denote each model prediction.

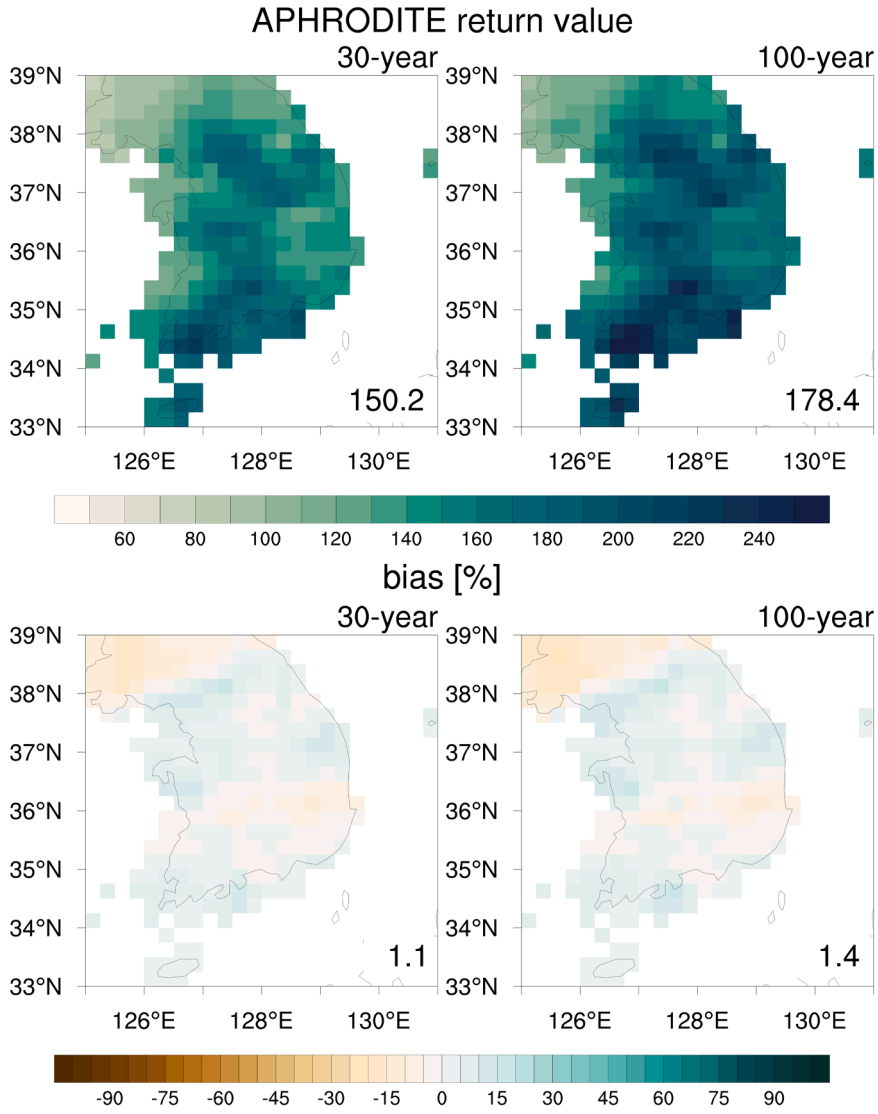

Fig. 5. The return values associated with 30- and 100-year return periods as in the observation (top row), and the difference [bias, %] between historical simulations and observation (bottom row). The return periods are indicated at the top of each panel.

historical values. Failure to do so could result in the flood defense systems which severely underestimate the magnitude and the frequency of the extreme events in the future.

4. Discussion

Extreme precipitation is projected to increase in the future, which is in agreement with previous studies that point to the intensification of precipitation over SK (Kim et al., 2018, 2020; Park et al., 2021). This intensification is consequence of changes in thermodynamics, dynamics and the precipitation efficiency in the changing climate. Namely in the case of SK, precipitation extremes are mostly connected to the East Asian Summer Monsoon rain band, of which increase has already been recorded (Li et al., 2023) and is projected to increase even more in the future (Katzenberger and Levermann, 2024), mainly due to increase in the large-scale water vapor rich environments in the warming climate.

However, extreme precipitation projections come with higher uncertainties than the projections of means, as well as different sources of uncertainty (Zhou et al., 2020; Hou et al., 2025). Namely, we have shown in previous research (Juzbašić et al., 2024) that the uncertainties in the variability of extreme precipitation projections for South Korea are more affected by scenario uncertainty than the projections of means are. Additionally, the uncertainty that comes from scenario differences is most pronounced in the southern part of SK, which is the area projected to experience higher increases in extreme precipitation. These uncertainties need to be taken into account when interpreting the results of this study and any similar studies.

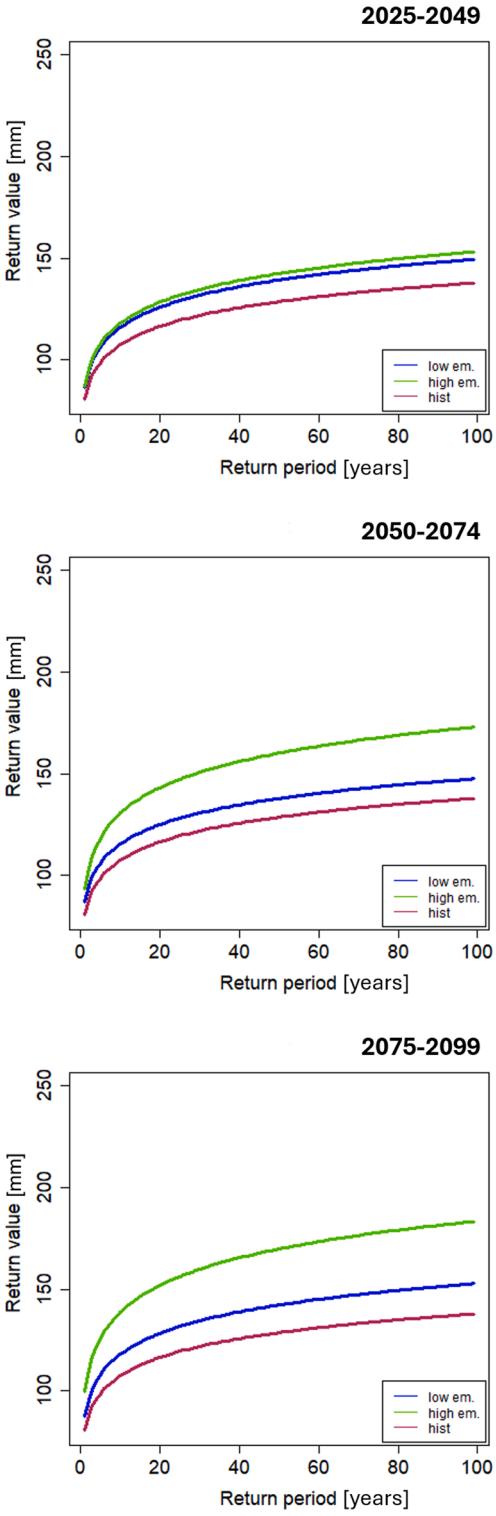

Fig. 6. Comparison of the simulated return periods for the three future periods - 2025–2049 (top), 2050–2074 (middle) and 2075–2099 (bottom). Historical values are marked in red color, low emissions in blue, and high emissions in green.

The present study indicates that the increases for the higher return periods are projected to be greater, which is most drastically visible at the end of the century in the high-emission scenario. That is, the value of RV100 is projected to increase the most, especially in the coastal regions. This is generally consistent with the conclusions of Kim et al. (2021), despite the different regional models,

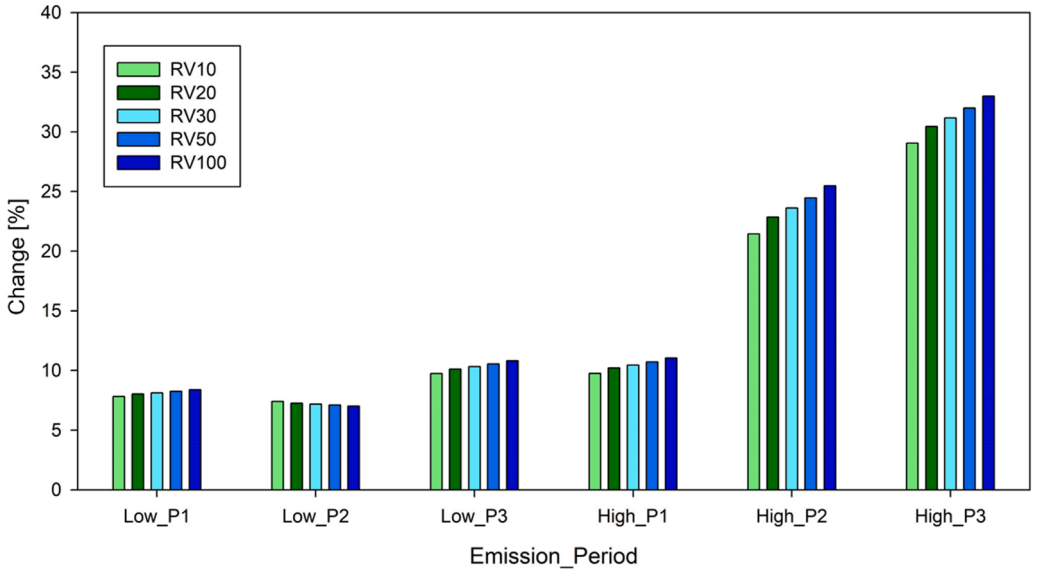

Fig. 7. Comparison of the increases (in %) of different return values depending on the time period and scenario analyzed. P1 indicates 2025–2049, P2 indicates 2050–2074 and P3 indicates 2075–2099 time period.

methodology, and bias correction methods, as well as the study conducted using CMIP6 CGCMs (Kim et al., 2025), which also concluded that future rainfall quantiles are expected to progressively increase.

While the probability of extreme events (100-year return values) is low, the high increase in the associated amounts raises serious concerns for flood and landslide risk. Additionally, not only are all the values associated with the return periods projected to increase, but the likelihood of events exceeding the return value thresholds is also projected to increase in the high-emission scenario. As the return values over all intervals are expected to increase, with a disproportionate increase in the larger return periods, our research underscores the importance of incorporating future climate projections into hazard planning. Kim et al. (2023), showed that for some of Korea's river basins, the future projected 100-year flood quantiles at the final exit points are higher than the historical 200-year flood quantile, which is consistent with the results of the present study, highlighting the importance of considering future projections in flood planning. Our study is also generally consistent with the conclusions of Moon et al. (2024), for the Seoul area, who also argue that the existing flood defense plans, which are grounded in historical observational data, are inadequate due to the anticipated increase in flooding in the future.

5. Conclusions

In the present study, simulations of precipitation extremes based on design frequencies over SK have been evaluated, and the possible future changes have been analyzed. The initial analysis showed that there are significant biases in each model simulation, which are somewhat lowered by using MME. However, as shown in Fig. 3, a relatively large bias can remain even after ensembling. Therefore, as accurate values are paramount for the projections of flooding risk and the building of flood defenses, as well as assessing the risk of landslides, bias correction is a necessity. Accordingly, the data have been bias-corrected using QDM as a method of correction. The analysis showed that QDM performed effectively, leaving a very minor remaining bias of under 3.5 % averaged over the SK domain, as well as bringing the interannual variability in line with the observations. In all future scenarios and periods, the amounts corresponding to return values for all return periods are projected to increase, but the amount of the increase depends largely on the level of emissions and the period analyzed. More extreme values are projected to increase even more in both magnitude and frequency, making it paramount to consider not just the historical observations but also the potential future precipitation.

There are, however, several limitations to this study. Firstly, the model resolution may still be too coarse for the area analyzed, given that the terrain of SK has many mountainous areas and the western and southern coasts are intricately indented. There are future simulations, both planned and currently ongoing, in which the model resolution will be increased further, allowing for better analysis of regional details. On a related note, while the present study focuses on changes in maximum daily precipitation, several recent studies have reported that sub-daily precipitation extremes may exhibit even larger changes than daily extremes (e.g., Zhang et al., 2022; Song et al., 2025, for China; Dallan et al., 2024, for Alpine-Mediterranean region, Crévolin et al., 2023, for Canada), underscoring the importance of examining finer temporal scales. Once the ongoing high-resolution simulations are completed, we plan to extend this analysis to include both finer spatial and temporal resolutions. Another limitation lies in the number of models and their realizations used. This study uses only 15 models and two scenarios, with only one ensemble member for each model. To gain a better understanding of the possible future changes, it would be beneficial to increase both the number of models and the number of ensemble members. Finally, the models used for these simulations were regional climate models. As such, they do not include direct feedback

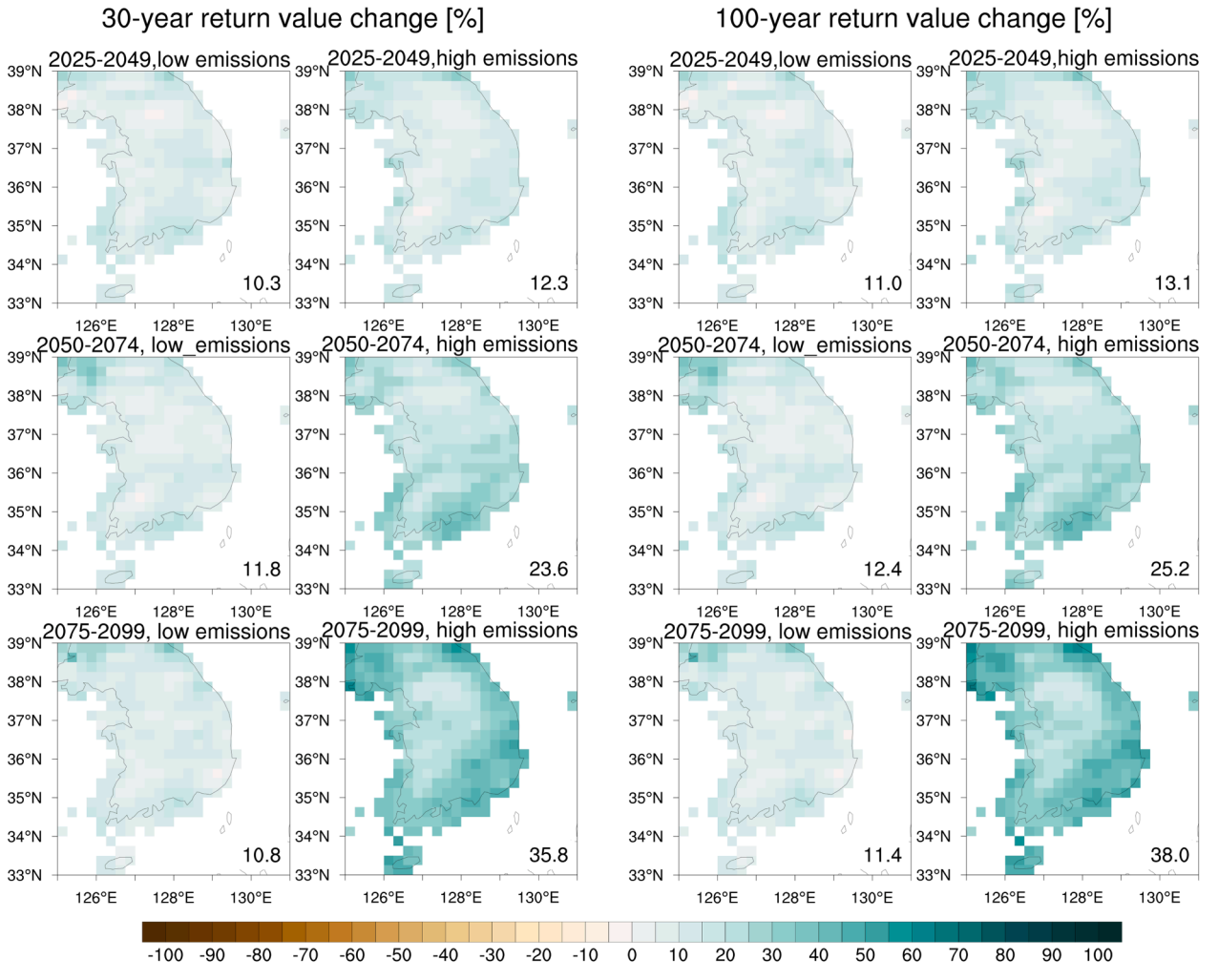

Fig. 8. The change [%] of the value associated with the 30-year(left) and 100-year (right) return periods as compared to historical simulation. The scenario and the future period are indicated above each panel.

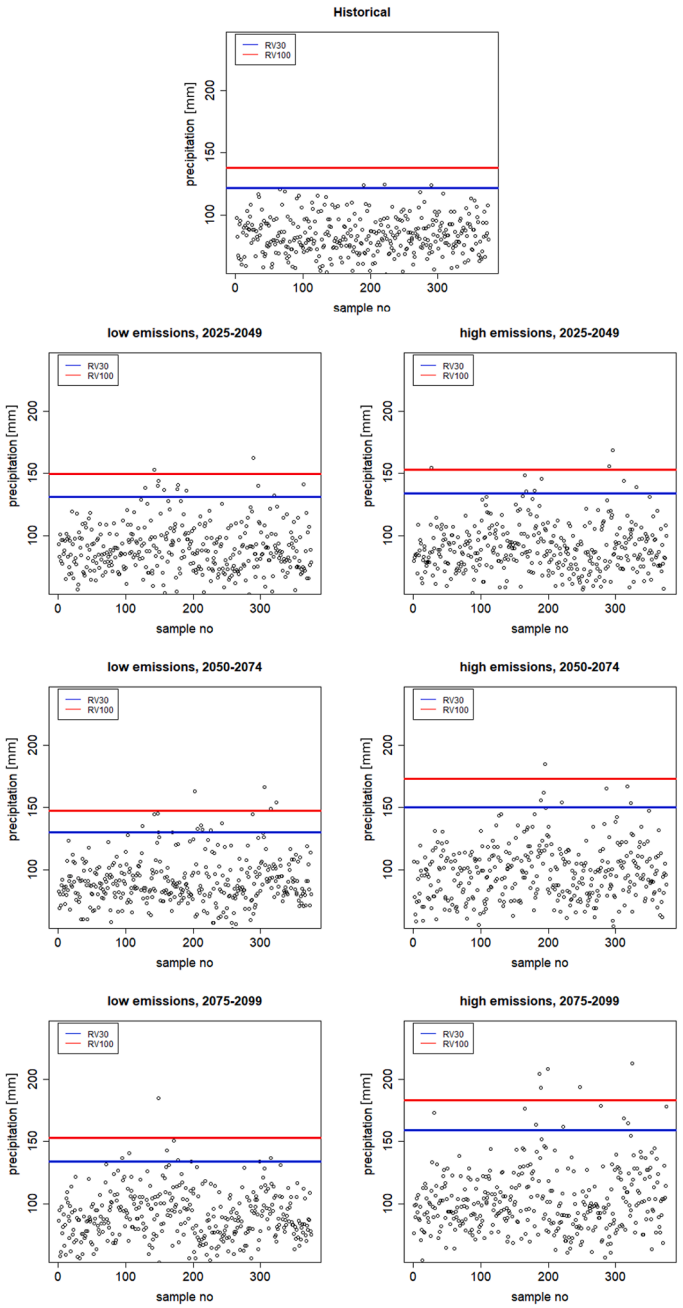

Fig. 9. The graph of all of the Rx1d samples, and how they compare to the return values of RV30 and RV100 associated with each period. Period and emission scenarios are indicated above each figure. Value of RV30 is marked in blue, and RV100 in red.

with aerosols. Therefore, to address this insufficiency, we plan to develop a regional Earth system model, which would include more complex feedback and thus provide a better simulation of realistic climate change.

This study highlights not only the importance of limiting emissions but also enacting the appropriate local adaptation policies on time. The analysis conducted in this study has demonstrated the benefits of utilizing high-resolution regional climate models for the projections of future extreme events. The present study can be utilized as a starting point for future analysis by impact modelers, risk assessment, future flood defense, agriculture, and city planning. Specifically, the flood defense systems and urban drain systems should be designed according to future projected return levels instead of historical ones, as this study has shown that the projected increases by the mid- and end-of-century periods can be quite significant. While structural design standards are typically based on 30- or 50-year return values derived from historical observations, considering the evolving distribution of precipitation extremes is essential to ensure the robustness of long-term infrastructure planning. Therefore, exclusively relying on historical data may lead to underestimation of

future precipitation, potentially resulting in avoidable damages.

CRediT authorship contribution statement

Seung-Ki Min: Writing – review & editing, Writing – original draft, Data curation. **Eun-Chul Chang:** Writing – review & editing, Writing – original draft, Data curation. **Youngeun Choi:** Writing – review & editing, Writing – original draft, Data curation. **Young-Hwa Byun:** Writing – review & editing, Writing – original draft, Data curation. **Changyong Park:** Writing – review & editing, Writing – original draft, Validation, Software, Methodology, Formal analysis, Conceptualization. **Ana Juzbašić:** Writing – review & editing, Writing – original draft, Visualization, Validation, Software, Methodology, Investigation, Formal analysis, Conceptualization. **Joong-Bae Ahn:** Writing – review & editing, Writing – original draft, Data curation. **Dong-Hyun Cha:** Writing – review & editing, Writing – original draft, Supervision, Funding acquisition, Conceptualization.

Declaration of Competing Interest

The authors declare that they have no known competing financial interests or personal relationships that could have appeared to influence the work reported in this paper.

Acknowledgements

This work was funded by the Korea Meteorological Administration Research and Development Program under Grant RS-2024–00403386.

This work was supported by Korea Environment Industry &Technology Institute(KEITI) through "Climate Change R&D Project for New Climate Regime.", funded by Korea Ministry of Environment(MOE) (2022003560002).

Data availability

Model data used in this study is available at https://esg-dn1.nsc.liu.se/search/cordex/. APHRODITE data used in this study is a published dataset (https://doi.org/10.1175/bams-d-11-00122.1), which is available at: https://www.chikyu.ac.jp/precip/english/downloads.html.

References

Baek, H., Kim, M., Kwon, W., 2017. Observed short- and long-term changes in summer precipitation over South Korea and their links to large-scale circulation anomalies. Int. J. Climatol. 37 (2), 972–986. https://doi.org/10.1002/joc.4753.

Beck, H.E., Zimmermann, N.E., McVicar, T.R., Vergopolan, N., Berg, A., Wood, E.F., 2018. Present and future Köppen–Geiger climate classification maps at 1-km resolution. Sci. Data 5, 180214. https://doi.org/10.1038/sdata.2018.214.

Cannon, A.J., Sobie, S.R., Murdock, T.Q., 2015. Bias correction of GCM precipitation by quantile mapping: how well do methods preserve changes in quantiles and extremes? J. Clim. 28 (17), 6938–6959. https://doi.org/10.1175/JCLI-D-14-00754.1.

Chen, C.A., Hsu, H.H., Liang, H.C., 2021. Evaluation and comparison of CMIP6 and CMIP5 model performance in simulating the seasonal extreme precipitation in the Western North Pacific and East Asia. Weather Clim. Extrem. 31. https://doi.org/10.1016/j.wace.2021.100303.

Choi, K.-S., Kim, B.-J., 2007. Climatological characteristics of tropical cyclones making landfall over the Korean peninsula. J. Korean Meteorol. Soc. 43, 97–109.

Ciarlo`, J.M., Coppola, E., Fantini, A., Giorgi, F., Gao, X., Tong, Y., Glazer, R.H., Torres Alavez, J.A., Sines, T., Pichelli, E., Raffaele, F., Das, S., Bukovsky, M., Ashfaq, M., Im, E.-S., Nguyen-Xuan, T., Teichmann, C., Remedio, A., Remke, T., Jacob, D., 2021. A new spatially distributed added value index for regional climate models: the EURO-CORDEX and the CORDEX-CORE highest resolution ensembles. Clim. Dyn. 57 (5–6), 1403–1424. https://doi.org/10.1007/s00382-020-05400-5.

Crévolin, V., Hassanzadeh, E., Bourdeau-Goulet, S.-C., 2023. Updating the intensity–duration–frequency curves in major Canadian cities under changing climate using CMIP5 and CMIP6 model projections. Sustain. Cities Soc. 92, 104473. https://doi.org/10.1016/j.scs.2023.104473.

Dallan, E., Marra, F., Fosser, G., Marani, M., Borga, M., 2024. Dynamical factors heavily modulate the future increase of sub-daily extreme precipitation in the Alpine–Mediterranean region. e2024EF005185 Earth'S. Future 12 (12). https://doi.org/10.1029/2024EF005185.

Davies, T., Cullen, M.J.P., Malcolm, A.J., Mawson, M.H., Staniforth, A., White, A.A., Wood, N., 2005. A new dynamical core for the met office's global and regional modelling of the atmosphere. Q. J. R. Meteorol. Soc. 131, 1759–1782.

Doms, G., Baldauf, M., 2013. A description of the nonhydrostatic regional COSMO-model Part I: Dynamics and Numerics. Tech. Rep. (COSMO—Consortium for Small-Scale Modelling.

Dunne, J.P., John, J.G., Adcroft, A.J., Griffies, S.M., Hallberg, R.W., Shevliakova, E., Stouffer, R.J., Cooke, W., Dunne, K.A., Harrison, M.J., Krasting, J.P., Malyshev, S. L., Milly, P.C.D., Phillipps, P.J., Sentman, L.T., Samuels, B.L., Spelman, M.J., Winton, M., Wittenberg, A.T., Zadeh, N., 2012. GFDL's ESM2 Global Coupled Climate–Carbon Earth System Models. Part I: Physical Formulation and Baseline Simulation Characteristics. J. Clim. 25 (19), 6646–6665. https://doi.org/10.1175/JCLI-D-11-00560.1.

Giorgetta, M.A., Jungclaus, J., Reick, C.H., Legutke, S., Bader, J., Böttinger, M., Brovkin, V., Crueger, T., Esch, M., Fieg, K., Glushak, K., Gayler, V., Haak, H., Hollweg, H., Ilyina, T., Kinne, S., Kornblueh, L., Matei, D., Mauritsen, T., Stevens, B., 2013. Climate and carbon cycle changes from 1850 to 2100 in MPI-ESM simulations for the Coupled Model Intercomparison Project phase 5. J. Adv. Model. Earth Syst. 5 (3), 572–597. https://doi.org/10.1002/jame.20038.

Giorgi, F., et al., 2012. RegCM4: model description and preliminary tests over multiple CORDEX domains Clim. Res 52, 7–29.

Gochis, D.J., et al., 2017. The weather research and forecasting model: overview, system efforts, and future directions Bull. Am. Meteorol. Soc. 98, 1717–1737.

Government of the Republic of Korea, 2020. Third National Climate Change Adaptation Plan (in Korean).

Grell, G.A., Dudhia, J., Stauffer, D., 1994. A description of the fifth-generation Penn State/NCAR mesoscale model (MM5). (University Corporation for Atmospheric Research).

Gumbel, E.J., 1941. The return period of flood flows. Ann. Math. Stat. 12 (2), 163–190.

Hong, S.-Y., et al., 2013. The global/regional integrated model system (GRIMs). Asia-Pac. J. Atmos. Sci. 49, 219–243.

Hou, R., Dai, P., Wu, R., Lin, Y., Li, Z., 2025. Assessing and reducing uncertainties in future mean and extreme precipitation projections over China. Atmos. Res. 326, 108301. https://doi.org/10.1016/j.atmosres.2025.108301.

Im, E.-S., Choi, Y.-W., Ahn, J.-B., 2017. Robust intensification of hydroclimatic intensity over East Asia from multi-model ensemble regional projections. Theor. Appl. Climatol. 129 (3–4), 1241–1254. https://doi.org/10.1007/s00704-016-1846-2.
IPCC, 2014. Climate Change 2014: Impacts, Adaptation, and Vulnerability. Part A: Global and Sectoral Aspects. Contribution of Working Group II to the Fifth Assessment Report of the Intergovernmental Panel on Climate Change.
IPCC, 2022. Climate Change 2022: Impacts, Adaptation, and Vulnerability. Contribution of Working Group II to the Sixth Assessment Report of the Intergovernmental Panel on Climate Change.
Jesus, L.F.L., Costa, V., Fernandes, W., 2020. Evaluating the influence of extending hydrologic time series in extreme quantile estimation. Water Environ. J. 34 (S1), 804–819. https://doi.org/10.1111/wej.12579.
Juzbašić, A., Park, C., Cha, D.-H., Ahn, J.-B., Chang, E.-C., Min, S.-K., Choi, Y., Byun, Y.-H., 2024. The difference in the uncertainty sources between future projections of mean and extreme precipitation over East Asia. Environ. Res. Lett. 19 (7), 074015. https://doi.org/10.1088/1748-9326/ad52ae.
Katz, R.W., Parlange, M.B., Naveau, P., 2002. Statistics of extremes in hydrology. Adv. Water Resour. 25 (8), 1287–1304. https://doi.org/10.1016/S0309-1708(02)00056-8.
Katzenberger, A., Levermann, A., 2024. Consistent increase in East Asian summer monsoon rainfall and its variability under climate change over China in CMIP6. Earth Syst. Dyn. 15 (4), 1137–1151. https://doi.org/10.5194/esd-15-1137-2024.
Kim, G., Cha, D.-H., Lee, G., Park, C., Jin, C.-S., Lee, D.-K., Suh, M.-S., Ahn, J.-B., Min, S.-K., Kim, J., 2020. Projection of future precipitation change over South Korea by regional climate models and bias correction methods. Theor. Appl. Climatol. 141 (3–4), 1415–1429. https://doi.org/10.1007/s00704-020-03282-5.
Kim, G., Cha, D., Park, C., Lee, G., Jin, C., Lee, D., Suh, M., Ahn, J., Min, S., Hong, S., Kang, H., 2018. Future changes in extreme precipitation indices over Korea. Int. J. Climatol. 38 (S1). https://doi.org/10.1002/joc.5414.
Kim, S., Joo, K., Kim, H., Shin, J.-Y., Heo, J.-H., 2021. Regional quantile delta mapping method using regional frequency analysis for regional climate model precipitation. J. Hydrol. 596, 125685. https://doi.org/10.1016/j.jhydrol.2020.125685.
Kim, S., Kwon, J.-H., Om, J.-S., Lee, T., Kim, G., Kim, H., Heo, J.-H., 2023. Increasing extreme flood risk under future climate change scenarios in South Korea. Weather Clim. Extrem. 39, 100552. https://doi.org/10.1016/j.wace.2023.100552.
Kim, S., Shin, J.-Y., Heo, J.-H., 2025. Assessment of future rainfall quantile changes in South Korea based on a CMIP6 multi-model ensemble. Water 17 (6), 894. https://doi.org/10.3390/w17060894.
KMA, 2021. Abnorm. Clim. Rep. 2020 (Korean).
Lee, J.-W., Hong, S.-Y., 2014. Potential for added value to downscaled climate extremes over Korea by increased resolution of a regional climate model. Theor. Appl. Climatol. 117 (3–4), 667–677. https://doi.org/10.1007/s00704-013-1034-6.
Lee, J.-H., Kim, S., Jang, S.-J., Kim, K., Cho, Y.-C., Kim, M., 2023. Preliminary analysis of a heavy rainfall–induced landslide on a slope with a photovoltaic power station in Hoengseong County, Gangwon Province, South Korea. Landslides 20 (8), 1763–1767. https://doi.org/10.1007/s10346-023-02077-9.
Lee, M., Min, S.-K., Cha, D.-H., 2023. Convection-permitting simulations reveal expanded rainfall extremes of tropical cyclones affecting South Korea due to anthropogenic warming. Npj Clim. Atmos. Sci. 6 (1), 176. https://doi.org/10.1038/s41612-023-00509-w.
Li, P., Song, F., Chen, H., Li, J., Prein, A.F., Zhang, W., Zhou, T., Zhuang, M., Furtado, K., Muetzelfeldt, M., Schiemann, R., Li, C., 2023. Intensification of mesoscale convective systems in the East Asian rainband over the past two decades. Geophys. Res. Lett. 50 (16), e2023GL103595. https://doi.org/10.1029/2023GL103595.
Li, Z., Sun, Y., Li, T., Ding, Y., Hu, T., 2019. Future Changes in East Asian Summer Monsoon Circulation and Precipitation Under 1.5–5 °C of Warming. Earth'S. Future 7 (12), 1391–1406. https://doi.org/10.1029/2019EF001276.
Lock, A.P., Brown, A.R., Bush, M.R., Martin, G.M., Smith, R.N.B., 2000. A new boundary layer mixing scheme. Part I: scheme description and single-column model tests *Mon.* Weather Rev 128, 3187–3199.
Martin, G.M., Bellouin, N., Collins, W.J., Culverwell, I.D., Halloran, P.R., Hardiman, S.C., Hinton, T.J., Jones, C.D., McDonald, R.E., McLaren, A.J., O'Connor, F.M., Roberts, M.J., Rodriguez, J.M., Woodward, S., Best, M.J., Brooks, M.E., Brown, A.R., Butchart, N., Dearden, C., Wiltshire, A., 2011. The HadGEM2 family of Met Office Unified Model climate configurations. Geosci. Model Dev. 4 (3), 723–757. https://doi.org/10.5194/gmd-4-723-2011.
Ministry of the Interior and Safety, 2023. 2022 Disaster Yearbook.
Moon, S., Ha, K.-J., 2020. Future changes in monsoon duration and precipitation using CMIP6. Npj Clim. Atmos. Sci. 3 (1), 45. https://doi.org/10.1038/s41612-020-00151-w.
Moon, H.-T., Yoon, S.-K., Kim, J.-S., Moon, Y.-I., 2024. Assessing future urban flood hazard: a comprehensive approach to estimating the implications of future rainfall scenarios. J. Flood Risk Manag. 17 (3), e13000. https://doi.org/10.1111/jfr3.13000.
Morrison, J.E., Smith, J.A., 2002. Stochastic modeling of flood peaks using the generalized extreme value distribution, 41-1-41–12 Water Resour. Res. 38 (12). https://doi.org/10.1029/2001WR000502.
National Geographic Information Institute, 2020. The National Atlas of Korea II. National Geographic Information Institute, Ministry of Land, Infrastructure and Transport.
Ngai, S.T., Tangang, F., Juneng, L., 2017. Bias correction of global and regional simulated daily precipitation and surface mean temperature over Southeast Asia using quantile mapping method. Glob. Planet. Change 149, 79–90. https://doi.org/10.1016/j.gloplacha.2016.12.009.
Nyaupane, N., Bhandari, S., Rahaman, Md.M., Wagner, K., Kalra, A., Ahmad, S., & Gupta, R. (2018). Flood Frequency Analysis Using Generalized Extreme Value Distribution and Floodplain Mapping for Hurricane Harvey in Buffalo Bayou. In *World Environmental and Water Resources Congress 2018* (pp. 364–375). https://doi.org/10.1061/9780784481400.034.
Park, C., Cha, D., Kim, G., Lee, G., Lee, D., Suh, M., Hong, S., Ahn, J., Min, S., 2020. Evaluation of summer precipitation over Far East Asia and South Korea simulated by multiple regional climate models. Int. J. Climatol. 40 (4), 2270–2284. https://doi.org/10.1002/joc.6331.
Park, C., Lee, G., Kim, G., Cha, D., 2021. Future changes in precipitation for identified sub-regions in East Asia using bias-corrected multi-RCMs. Int. J. Climatol. 41 (3), 1889–1904. https://doi.org/10.1002/joc.6936.
Park, C., Min, S.-K., 2019. Multi-RCM near-term projections of summer climate extremes over East Asia. Clim. Dyn. 52 (7–8), 4937–4952. https://doi.org/10.1007/s00382-018-4425-7.
Park, C., Moon, J.-Y., Cha, E.-J., Yun, W.-T., Choi, Y., 2008. Recent changes in summer precipitation characteristics over South Korea. J. Korean Geogr. Soc. 45, 324–336 (in Korean with English abstract).
Park, C., Shin, S.-W., Cha, D.-H., Suh, M.-S., Hong, S.-Y., Ahn, J.-B., Min, S.-K., Byun, Y.-H., 2022. Future Projections of Precipitation using Bias–Corrected High–Resolution Regional Climate Models for Sub–Regions with Homogeneous Characteristics in South Korea. AsiaPac. J. Atmos. Sci. 58 (5), 715–727. https://doi.org/10.1007/s13143-022-00292-3.
Qin, X., Dai, C., 2022. Comparison of different quantile delta mapping schemes in frequency analysis of precipitation extremes over mainland Southeast Asia under climate change. J. Hydrol. 606, 127421. https://doi.org/10.1016/j.jhydrol.2021.127421.
Sellar, A.A., Jones, C.G., Mulcahy, J.P., Tang, Y., Yool, A., Wiltshire, A., O'Connor, F.M., Stringer, M., Hill, R., Palmieri, J., Woodward, S., de Mora, L., Kuhlbrodt, T., Rumbold, S.T., Kelley, D.I., Ellis, R., Johnson, C.E., Walton, J., Abraham, N.L., Zerroukat, M., 2019. UKESM1: Description and Evaluation of the U.K. Earth System Model. J. Adv. Model. Earth Syst. 11 (12), 4513–4558. https://doi.org/10.1029/2019MS001739.
Seo, G., Ahn, J., Cha, D., Suh, M., Min, S., Chang, E., Byun, Y., Kim, J., 2023. Evaluation of multi-RCMensembles for simulating spatiotemporal variability of Asian summer monsoon precipitation in the CORDEX-East Asia Phase 2 domain. Int. J. Climatol. 43 (8), 3710–3729. https://doi.org/10.1002/joc.8054.
Seoul Metropolitan Government, 2014. Supplementary Investigation Report on the Causes of the Mt. Umyeon Landslide (in Korean).
Smith, R.N.B., 1990. A scheme for predicting layer clouds and their water content in a general circulation model. Q. J. R. Meteorol. Soc. 116, 435–460.
Song, L., Yan, L., Chai, F., Lu, F., Zhai, J., Luan, Q., Ma, Q., Jiang, C., Zhang, M., Sun, J., 2025. Future projections of the rainfall intensity–duration–frequency curves in the Beijing–Tianjin–Hebei urban agglomeration based on NEX-GDDP CMIP6 simulations. Sustain. Cities Soc. 121, 106227. https://doi.org/10.1016/j.scs.2025.106227.
Sung, J.H., Kang, D.H., Seo, Y.-H., Kim, B.S., 2023. Analysis of Extreme Rainfall Characteristics in 2022 and Projection of Extreme Rainfall Based on Climate Change Scenarios. Water 15 (22), 3986. https://doi.org/10.3390/w15223986.

Torma, C., Giorgi, F., Coppola, E., 2015. Added value of regional climate modeling over areas characterized by complex terrain—Precipitation over the Alps. J. Geophys. Res. Atmospheres 120 (9), 3957–3972. https://doi.org/10.1002/2014JD022781.

Vangelis, H., Zotou, I., Kourtis, I.M., Bellos, V., Tsihrintzis, V.A., 2022. Relationship of Rainfall and Flood Return Periods through Hydrologic and Hydraulic Modeling. Water 14 (22). https://doi.org/10.3390/w14223618.

Yatagai, A., Kamiguchi, K., Arakawa, O., Hamada, A., Yasutomi, N., Kitoh, A., 2012. APHRODITE: constructing a long-term daily gridded precipitation dataset for Asia Based on a dense network of rain gauges. Bull. Am. Meteorol. Soc. 93 (9), 1401–1415. https://doi.org/10.1175/BAMS-D-11-00122.1.

Zhang, B., Wang, S., Moradkhani, H., Slater, L., Liu, J., 2022. A vine copula-based ensemble projection of precipitation intensity–duration–frequency curves at sub-daily to multi-day time scales. e2022WR032658 Water Resour. Res. 58 (11). https://doi.org/10.1029/2022WR032658.

Zhou, T., Lu, J., Zhang, W., Chen, Z., 2020. The sources of uncertainty in the projection of global land monsoon precipitation. e2020GL088415 Geophys. Res. Lett. 47 (14). https://doi.org/10.1029/2020GL088415.